CNSNS 249
8 March 2005 Disk Used
ARTICLE IN PRESS
No. of Pages 18, DTD = 5.0.1

Available online at www.sciencedirect.com
SCIENCE DIRECT®
Communications in Nonlinear Science and Numerical Simulation xxx (2005) xxx–xxx
Communications in Nonlinear Science and Numerical Simulation
www.elsevier.com/locate/cnsns

The second law of thermodynamics and multifractal distribution functions: Bin counting, pair correlations, and the Kaplan–Yorke conjecture

Wm.G. Hoover [a,*], C.G. Hoover, H.A. Posch [b], J.A. Codelli [a]

[a] *Department of Applied Science, University of California at Davis/Livermore and Lawrence Livermore National Laboratory Livermore, CA 94551-7808, USA*
[b] *Institute for Experimental Physics, University of Vienna, Boltzmanngasse 5, Vienna A-1090, Austria*

Received 7 February 2005; received in revised form 9 February 2005; accepted 9 February 2005

Abstract

We explore and compare numerical methods for the determination of multifractal dimensions for a doubly-thermostatted harmonic oscillator. The equations of motion are continuous and time-reversible. *At* equilibrium the distribution is a four-dimensional Gaussian, so that all the dimension calculations can be carried out analytically. *Away from* equilibrium the distribution is a surprisingly isotropic multifractal strange attractor, with the various fractal dimensionalities in the range $1 < D < 4$. The attractor is relatively homogeneous, with projected two-dimensional information and correlation dimensions which are nearly independent of direction. Our data indicate that the Kaplan–Yorke conjecture (for the information dimension) fails in the full four-dimensional phase space. We also find no plausible extension of this conjecture to the *projected* fractal dimensions of the oscillator. The projected growth rate associated with the largest Lyapunov exponent is *negative* in the one-dimensional coordinate space.

PACS: 02.70.Ns; 05.20.−y; 05.770.Ln; 07.05.Tp

Keywords: Fractal dimensions; Nonlinear dynamics; Kaplan–Yorke dimension

* Corresponding author. Tel.: +1 775 779 2219; fax: +1 925 422 8681.
E-mail address: hooverwilliam@yahoo.com (Wm.G. Hoover).

1007-5704/$ - see front matter
doi:10.1016/j.cnsns.2005.02.002

1. Introduction

In 1983, Shuichi Nosé discovered a deterministic and time-reversible thermostatted dynamics capable of imposing a time-averaged kinetic temperature $\langle T \rangle$ on selected degrees of freedom [1,2]. His dynamics was both time-reversible and deterministic, but could nevertheless be used to model irreversible behavior. The most useful form of his dynamics has been called "Nosé–Hoover dynamics", after the studies of a thermostatted harmonic oscillator inspired by Nosé's work [3,4].

In 1987 related studies of the Galton Board [5] and Galton Staircase [6] models showed that *nonequilibrium* stationary states generated with time-reversible motion equations generate multifractal phase-space distributions [5–8]. A typical sample, from the Galton Board studies, is shown in Fig. 1. A dynamical analysis, through the Lyapunov spectrum, shows how symmetry breaking, through dynamical instability, results in trajectories obeying the Second Law of Thermodynamics. The motion *forward* in time is more stable (smaller Lyapunov exponents) than is the reversed motion *backward* in time. The resulting fractal distributions thus provide a simple resolution of the Loschmidt paradox, which contrasts the one-way Second Law of Thermodynamics with the either-way nature of time-reversible microscopic dynamics [6,9].

Here we investigate a prototypical nonequilibrium problem which generates a multifractal strange attractor in its (four-dimensional) phase space. The adjective "Multifractal" signifies that the apparent dimensionality of the attractor (the number of attractor points lying within a distance r is proportional to r^D) varies from point to point, making it possible to define whole families of fractal dimensions. Measures proportional to different powers of the phase-space probability density emphasize different regions of the attractor, giving rise to different characteristic overall dimensionalities. The dimensionalities of the nonequilibrium fractal distributions are

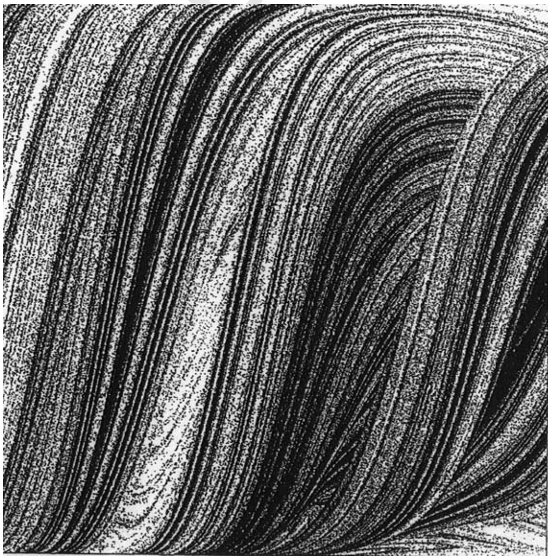

Fig. 1. Phase plane for the Galton Board problem. The 10^6 points shown here represent successive collisions of a point particle in an infinite periodic array of hard-disk scatterers. For details see Ref. [5].

all less than those of the corresponding equilibrium distribution, typically by an amount proportional to the rate of entropy production [9–13].

Much more recently, numerical studies of the many-body thermal conductivity for the ϕ^4 potential model—a crystal with harmonic interactions and quartic tethers of particles to sites—revealed that the nonequilibrium dimensionality loss can be quite large. The calculated dimensionality losses for the ϕ^4 model systems agreed nicely with predictions based on simple ideas from chaotic dynamics and irreversible thermodynamics [14–17]. Posch and Hoover estimated the dimensionality reduction in the subspace of the purely Hamiltonian degrees of freedom in ϕ^4 systems with a few hundred degrees of freedom. This work, based on a large-system extension of the Kaplan–Yorke conjecture, quantified the dimensionality reduction that can occur in Hamiltonian phase spaces far from equilibrium. We were motivated to test these same ideas for the small system studied here.

The realization that multifractal distribution functions are commonplace in nonequilibrium systems has led to the creation and exploration of many simple models. Among these, the doubly-thermostatted harmonic oscillator has unique properties. Unlike maps and hard-particle models, the oscillator trajectory is smooth everywhere, free of any singularities. Near equilibrium the distribution is ergodic and analytic, tracing out a four-dimensional Gaussian probability density in the full phase space. Away from equilibrium the oscillator control equations can be designed to obey either of the thermodynamic identities,

$$\langle T\mathrm{d}S_{\mathrm{ext}}/\mathrm{d}t\rangle \equiv \langle -\mathrm{d}Q/\mathrm{d}t\rangle$$

or

$$\langle \mathrm{d}S_{\mathrm{ext}}/\mathrm{d}t\rangle \equiv \langle -(1/T)\mathrm{d}Q/\mathrm{d}t\rangle,$$

where Q is the heat transferred to the oscillator at the temperature T and S_{ext} is the external entropy. Both T and S_{ext} vary with time. The angular brackets indicate long-time averages. These heat-transfer relations follow directly from the chosen thermostatted equations of motion, as we see in detail in Section 3. The second of them leads directly to Clausius' form of the Second Law of Thermodynamics [18]:

$$\langle \mathrm{d}S_{\mathrm{ext}}/\mathrm{d}t\rangle \equiv \langle -(1/T)\mathrm{d}Q/\mathrm{d}t\rangle > 0,$$

where the time average has to be taken over many successive realizations of a cyclic irreversible process.

It is difficult to conceive of a simpler set of deterministic time-reversible flow equations which still exhibits all the qualitative features of more complicated many-body stationary states. We discuss and apply algorithms for determining the multifractal dimensions of the nonequilibrium oscillator's strange attractor, both in the full four-dimensional phase-space and in its various subspaces. The various multifractal dimensions characterizing nonequilibrium attractors vary smoothly from the full phase-space dimension down to unity as the departure from equilibrium is increased.

The remainder of this paper is organized as follows: in Section 2 the *equilibrium* isothermal oscillator is considered. Its dynamics generates a four-dimensional Gaussian distribution in phase space. This special case makes it possible to test our numerical algorithms against known analytic results. A *nonequilibrium* version of this oscillator is described in Section 3, with the connection to irreversible thermodynamics discussed in Section 4. Detailed numerical results for this nonequilibrium case are given in Section 5. The extension of the equilibrium case considered there uses a simple hyperbolic tangent relation linking the thermodynamic temperature to the oscillator coordinate. Section 6 explores the applicability of Kaplan and Yorke's ideas to multifractal dimensions in both the full phase space and its subspaces. Section 7 is devoted to the conclusions gleaned from this work.

2. Gaussian phase-space distributions

At equilibrium a simple model for the phase-space distribution is a many-dimensional Gaussian, with the probability density for a typical phase-space variable x given by the normalized Gaussian function

$$\sqrt{2\pi}g(x) \equiv \mathrm{e}^{-x^2/2}.$$

The *four*-dimensional version of this distribution, with phase-space variables (q, p, ζ, ξ), is

$$f(q, p, \zeta, \xi) \equiv g(q)g(p)g(\zeta)g(\xi).$$

It can be generated by the long-time-average trajectory from the set of four ordinary differential equations describing a doubly-thermostatted oscillator. For simplicity we write the equations here in the most basic possible form, with each of the several arbitrary parameters set equal to unity:

$$\dot{q} = p; \quad \dot{p} = -q - \zeta p - \xi p^3;$$

$$\dot{\zeta} = p^2 - 1; \quad \dot{\xi} = p^4 - 3p^2.$$

Nonequilibrium generalizations are discussed in the following Sections. For additional examples, see Ref. [10]. Here, the oscillator coordinate is q. The momentum is p. The two control variables, or "friction coefficients", are ζ and ξ. They control, respectively, the second and fourth moments of the momentum distribution, $\langle p^2 \rangle$ and $\langle p^4 \rangle$. These four ordinary differential equations generate the full four-dimensional Gaussian distribution in (q, p, ζ, ξ) space:

$$(2\pi)^2 f(q, p, \zeta, \xi) = \exp\left[-\frac{1}{2}(q^2 + p^2 + \zeta^2 + \xi^2)\right].$$

The normalization constant $(2\pi)^2$ follows from the four-dimensional definite integral:

$$\int_{-\infty}^{+\infty}\int_{-\infty}^{+\infty}\int_{-\infty}^{+\infty}\int_{-\infty}^{+\infty} f(q, p, \zeta, \xi)\mathrm{d}q\,\mathrm{d}p\,\mathrm{d}\zeta\,\mathrm{d}\xi \equiv 1.$$

Fig. 2 indicates how the smooth four-dimensional Gaussian distribution develops from the patently one-dimensional trajectory. It is a projection of the motion into the two-dimensional (q, p) subspace. Each view of the projection consists of 200,000 separate points, with successive points separated in time by 0.1, 1.0, 10.0, and 100.0. (The correlation time for the system is of the order of the unconstrained oscillator period, 2π, as is indicated by the Lyapunov spectrum discussed in Section 5 below). In the following Section we detail the modifications necessary to treat nonequilibrium systems with a variable temperature, $T = T(q)$.

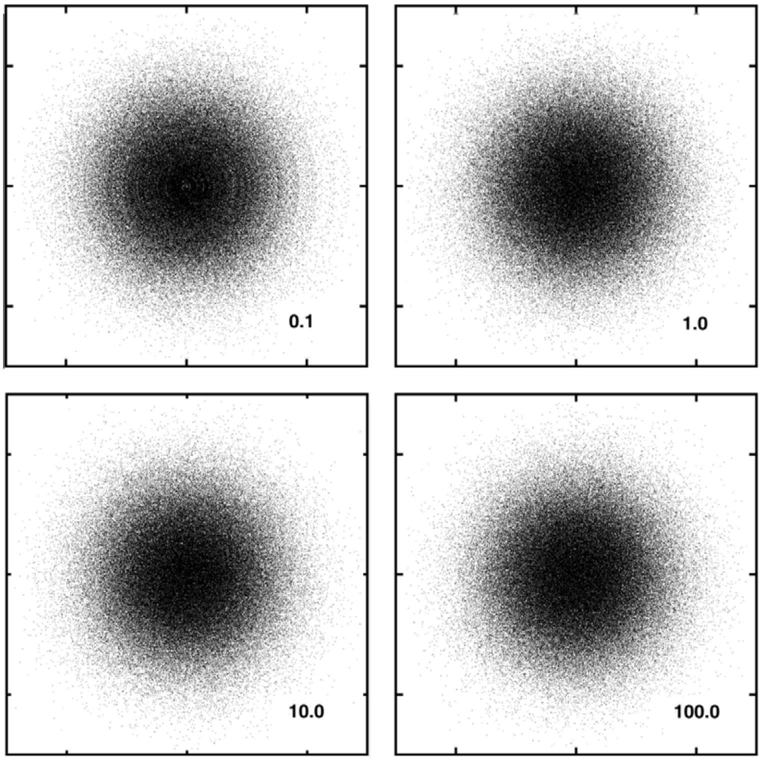

Fig. 2. Development of the $\{q,p\}$ distribution function at equilibrium, where the final distribution is a Gaussian, $\propto \exp[\frac{-1}{2}(q^2+p^2)]$. Each of the four plots shows 200,000 points. The separations between successive points are 0.1, 1.0, 10.0, 100.0. The lack of any significant difference between the last two sets of points suggests (in agreement with the Lyapunov spectrum) that correlations are lost after a time of order 10–100. The abscissa and ordinate ranges are both ± 4.

3. Nonequilibrium equations of motion

Now let us include explicitly all of the arbitrary parameters, still for a single harmonic oscillator with coordinate q and momentum p. Then the *non*equilibrium equations of motion we study here have the form:

$$\dot{q} = p/m; \quad \dot{p} = -\kappa q - \zeta p - \xi p(p^2/mkT_0);$$
$$\dot{\zeta} = [(p^2/mkT_0) - (T/T_0)]/\tau^2;$$
$$\dot{\xi} = [(p^2/mkT_0)^2 - 3(p^2/mkT_0)(T/T_0)]/\tau^2.$$

Here the coordinate-dependent temperature $T = T(q)$ is distinguished from the constant value T_0. We choose a particular form for the coordinate dependence of T so that the reduced temperature T/T_0 varies from $1-\epsilon$ (as $q/h \to -\infty$) to $1+\epsilon$ (as $q/h \to +\infty$):

$$T/T_0 = T(q)/T_0 = 1 + \epsilon \tanh(q/h).$$

The mass and force constant of the oscillator are m and κ; k is Boltzmann's constant, and τ is a relaxation time. In the event that ϵ is nonzero, the oscillator is exposed to a temperature gradient. For a long-time-averaged simulation (several oscillator vibrations) heat will flow against the direction of the temperature gradient. The resulting dissipation generates a steady stationary state of the system: a strange attractor in the four-dimensional phase space. Several special cases of such multifractal attractors are discussed in Ref. [10]. In the remainder of the paper we consider the following special case:

$$m = 1; \quad \kappa = 1; \quad k = 1;$$
$$T_0 = 1; \quad \tau = 1; \quad \epsilon = 1; \quad h = 1.$$

4. Thermodynamic relations from phase-space time averages

The energy of the thermostatted oscillator changes in time, due to the nonHamiltonian force $-\zeta p - \xi p^3$. As is usual in thermodynamics, we use $\mathrm{d}Q/\mathrm{d}t$ to indicate the heat transferred *to* the oscillator *from* the thermodynamic thermostats. We would expect to find that the time-averaged value $\langle (1/T)\mathrm{d}Q/\mathrm{d}t\rangle$ is negative, reflecting the dissipation induced in the external reservoirs through the coordinate-dependent temperature. At the same time, in any stationary state with no work done the total time-averaged heat transfer must vanish:

$$\langle \mathrm{d}Q/\mathrm{d}t\rangle = \langle -\zeta p^2 - \xi p^4\rangle = 0,$$
$$\langle (1/T)\mathrm{d}Q/\mathrm{d}t\rangle = \langle (-\zeta p^2 - \xi p^4)/T\rangle < 0.$$

For this oscillator there is no equivalence between the time-averaged rate of external entropy production, $\langle \mathrm{d}S_{\mathrm{ext}}/\mathrm{d}t\rangle$, and the loss of phase volume, $\langle \mathrm{d}\ln\otimes/\mathrm{d}t\rangle$:

$$\langle \mathrm{d}S_{\mathrm{ext}}/\mathrm{d}t\rangle = \langle -(1/T)\mathrm{d}Q/\mathrm{d}t\rangle \simeq 0.093;$$
$$\langle \mathrm{d}\ln\otimes/\mathrm{d}t\rangle = -\langle \mathrm{d}\ln f/\mathrm{d}t\rangle \simeq 0.440.$$

It is easy to calculate the difference between the two:

$$(1/T)\mathrm{d}Q/\mathrm{d}t = -\mathrm{d}\ln f/\mathrm{d}t - (1/2T)\mathrm{d}/\mathrm{d}t(\zeta^2 + \xi^2).$$

Even so, we have chosen to study the present model in detail, rather than some of the many alternatives considered in Ref. [10] and the alternative discussed just below, because the present model has a particularly interesting fractal structure in its phase space and provides also a stringent test of the Kaplan–Yorke conjecture discussed later.

A direct link with thermodynamics *can* be forged by solving the alternative set of motion equations:

$$\dot{q} = p; \quad \dot{p} = -q - \zeta p - \xi(p^3/T);$$
$$\dot{\zeta} = [(p^2/T) - 1]/\tau^2; \quad \dot{\xi} = [(p^4/T^2) - 3(p^2/T)]/\tau^2,$$
$$T = T(q) = 1 + \epsilon\tanh(q/h).$$

In this case the heat transfer to the oscillator, divided by kT, has a time-averaged value exactly matching the dissipation rate, as seen through the loss of phase volume:

$$\langle(1/kT)\mathrm{d}Q/\mathrm{d}t\rangle = \langle-\zeta(p^2/T) - \xi(p^4/T^2)\rangle = \langle-\zeta - 3\xi(p^2/T)\rangle = \langle\mathrm{d}\ln\otimes/\mathrm{d}t\rangle = -\langle\mathrm{d}\ln f/\mathrm{d}t\rangle.$$

Beyond checking that this model too has a stationary dissipative state for $\epsilon = \tau = h = 1$, similar to the one studied in detail here, but less far from equilibrium (higher fractal dimensions) and therefore geometrically less interesting, we have carried out only limited investigations of this model. *At* equilibrium, for any of these models, the phase-space probability density for a fixed constant T and τ is:

$$(T/\tau^2)(2\pi)^2 f(q,p,\zeta,\xi) = \exp\left[-\frac{1}{2T}(q^2+p^2)\right]\exp\left[-\frac{\tau^2}{2}(\zeta^2+\xi^2)\right],$$

The equilibrium thermodynamic identity that results is:

$$\langle(\mathrm{d}Q/\mathrm{d}t)/T\rangle = \langle(-\zeta - 3p^2\xi)/T\rangle = \langle-\mathrm{d}S_{\mathrm{ext}}/\mathrm{d}t\rangle.$$

In the corresponding nonequilibrium case, where the temperature is a given function of the coordinate rather than constant, $T = T(q)$, any of these models must necessarily satisfy the Second Law of Thermodynamics, with f diverging on a multifractal strange attractor and with the time-averaged entropy production $\langle\mathrm{d}S_{\mathrm{ext}}/\mathrm{d}t\rangle$ strictly positive. Because a stationary state can be viewed as many repetitions of a cyclic irreversible process the exact relation which results for the second of the models is

$$\langle(\mathrm{d}Q/\mathrm{d}t)/T\rangle = \langle-\mathrm{d}S_{\mathrm{ext}}/\mathrm{d}t\rangle < 0.$$

This time-averaged result is exactly Clausius' form of the Second Law of Thermodynamics [18].

5. Multifractal dimensions via bin counting, pair correlations, and the Kaplan–Yorke conjecture

In the simplest *non*equilibrium case, with $(m,k,\kappa,T_0,\tau,\epsilon,h)$ all equal to unity, and

$$0 < T(q) = 1 + \tanh(q) < 2,$$

the stationary distribution still occupies the same four-dimensional phase space as at equilibrium, but the information dimension D_{I}, along with the Kaplan–Yorke dimension D_{KY}, (defined by a vanishing Lyapunov sum detailed later in this section) drops below the equilibrium value,

$$D_{\mathrm{KY}} \simeq D_{\mathrm{I}} = D_1 < D_{\mathrm{eq}} = 4.$$

Nonequilibrium distributions for this example, projected into the six two-dimensional planes, (q,p), (q,ζ), (q,ξ), (p,ζ), (p,ξ), and (ζ,ξ), make up Fig. 3.

Fig. 4 shows how the fractal distribution develops in the (ζ,ξ) plane, as the sampling time between successive points is increased. The figure shows 200,000 points, projected into the (ζ,ξ) plane, with sampling intervals of 0.001, 0.01, 0.1, 1.0, and 10.0. The appearance of these fractal distributions is qualitatively different to that of the smooth Gaussian distribution which is the equilibrium solution. A variety of fractal dimensions have been defined in order to characterize such nonequilibrium systems.

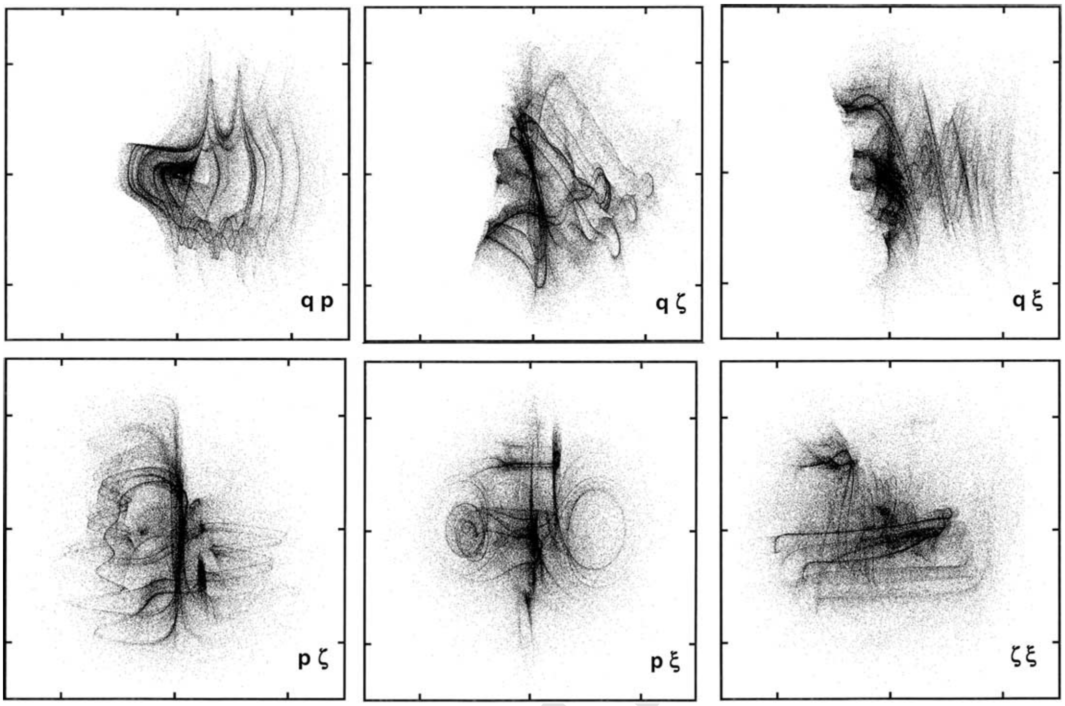

Fig. 3. Projections (200,000 points each) of the nonequilibrium $qp\zeta\xi$ oscillator dynamics into six phase-space subspaces: $\{qp, q\zeta, q\xi, p\zeta, p\xi, \zeta\xi\}$. The time separation between successive points is 10.0. The abscissa and ordinate ranges are both ± 6 for these projections.

The multifractal dimensions D_0, D_1, D_2, $D_3, \ldots$ can all be computed from the moments (or measures) associated with phase-space boxes or "bins". For the jth bin, the various measures are $\{\mu_p\}$:

$$\mu_p(j) \equiv N_j^p \Big/ \sum_k N_k^p,$$

where the $\{N_k\}$ are the number of observed points (proportional to the probability) in the kth bin. If the bins have a characteristic size Δ then the multifractal dimensions correspond to the limiting slopes of the plots of $\langle \ln \mu_p \rangle$ versus $\ln \Delta$. For ergodic systems a sufficiently long trajectory eventually reaches *all* bins. In such a case the measure μ_0 is uniform. For other values of p the measure is concentrated in a characteristic part of the attractor. Fig. 5 shows the variation of the measures' above-average-probability "cores" for the nonequilibrium oscillator. Because the measures μ_0 and μ_3 are relatively slow to converge, in our numerical work we concentrate on the information and correlation dimensions derived from μ_1 and μ_2.

Chhabra and Jensen [19] developed an equivalent, but more direct approach to the determination of the multifractal dimensions. They showed that the various multifractal dimensions $\{D_q\}$ were given by the simple set of small-bin-size limits ($\Delta \to 0$):

$$D_q = \left(\sum \mu_q \ln \mu_q \right) \Big/ \ln \Delta.$$

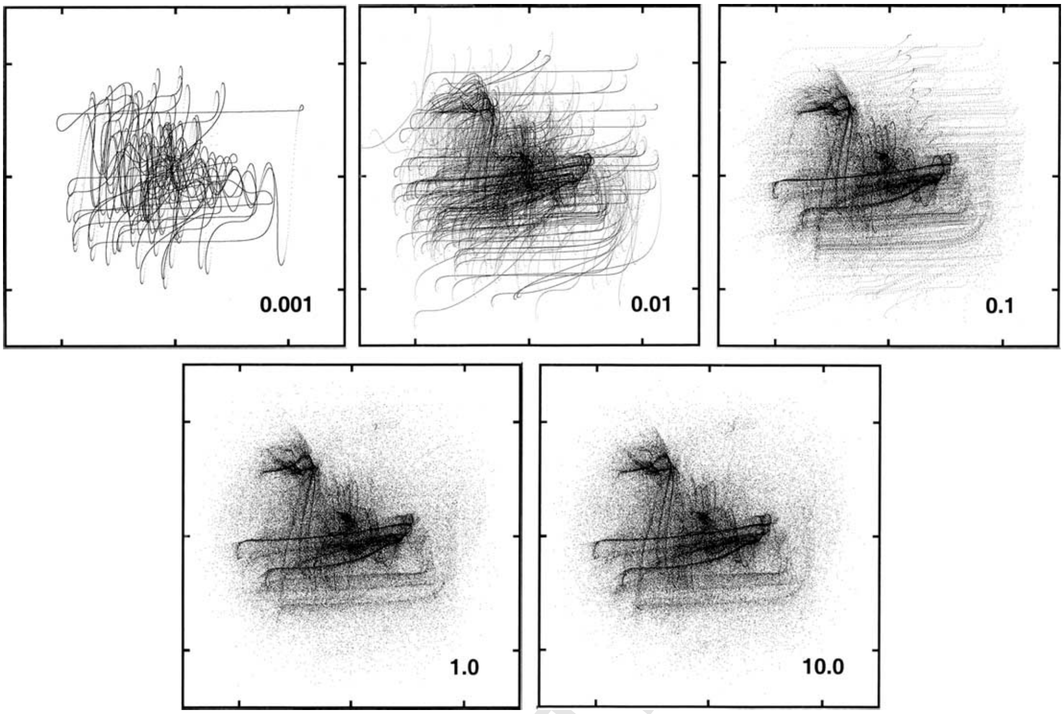

Fig. 4. Development of the nonequilibrium $\{\zeta, \xi\}$ distribution function. Each of the five plots shows 200,000 points. The separations between successive points are 0.001, 0.01, 0.1, 1.0, and 10.0. The lack of any significant difference between the last two sets of points suggests (in agreement with the Lyapunov spectrum) that correlations are lost after a time of order 10–100. The abscissa and ordinate ranges are both ±6 for these plots.

It is also possible to define generalized dimensions by using two *different* measures, q_1 and q_2:

$$D_{(q_1,q_2)} = \left(\sum \mu_{q_1} \ln \mu_{q_2}\right) \Big/ \ln \Delta.$$

The usual $f(\alpha)$ relation linking fractal dimension f to singularity strength α uses $q_1 = q_2$ for $f(q) \equiv D_{(q,q)}$ and $q_1 = 1$ for $\alpha(q) \equiv D_{(1,q)}$ [19].

With presentday computers it is inconvenient to consider a four-dimensional grid with a substantially higher resolution than

$$128 \times 128 \times 128 \times 128 = 2^{28} = 268,435,456$$

phase-space bins. Both storage capacity, as well as the need to generate an average of *several* points per bin (with successive points separated by 10^3 or 10^4 timesteps to avoid serial correlation) combine to make this four-dimensional problem a severe computational challenge. We carried out this stage of refinement by dividing up the grid data among storage files. The three-dimensional subspaces are simpler to treat. A resolution of 512 bins in each of three directions requires arrays half the size (2^{27} bins) of the four-dimensional ones considered here.

Because (according to the Kaplan–Yorke conjecture discussed below) the nonequilibrium information dimension is less than three for the special case chosen here: $D_1 \simeq D_{\mathrm{KY}} = 2.80 < 3$, we

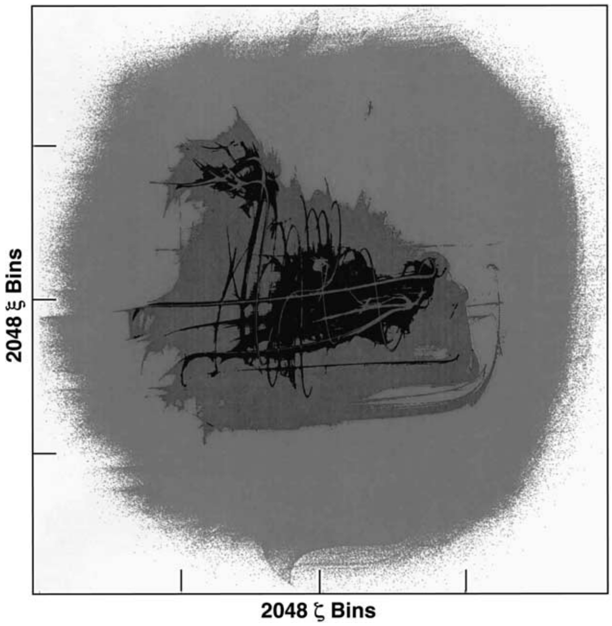

Fig. 5. Successively smaller attractor cores are shown here, projected into $\{\zeta, \xi\}$ space. They correspond, in order of decreasing size, to the "bin-counting", "information", "correlation", and "three-point" dimensions. The "cores" correspond to those bins (on a 2048×2048 grid) with above average probability, where the bin probabilities are proportional to $N_k^{0.1}$, N_k^1, N_k^2, and N_k^3 for the three cases. One billion data points, separated by 100 timestep intervals, were used in constructing this figure.

expect to glean significant information by comparing nonequilibrium and equilibrium studies carried out in the various subspaces:

$$\{(q,p,\zeta),(q,p,\xi),(q,\zeta,\xi),(p,\zeta,\xi)\},$$
$$\{(q,p),(q,\zeta),(q,\xi),(p,\zeta),(p,\xi),(\zeta,\xi)\},$$
$$\{(q),(p),(\zeta),(\xi)\}.$$

In the full four-dimensional phase space, the information dimension $D_I = D_1$ can be estimated independently of bin counting. Kaplan and Yorke conjectured that $D_{\mathrm{KY}} \simeq D_I$ can be estimated from the Lyapunov spectrum. D_{KY} corresponds to the number of Lyapunov exponents (starting with the largest) for which the sum $\sum \lambda_i$ vanishes. Typically the sum has to be linearly interpolated.

In the equilibrium case ϵ vanishes and the temperature is constant. If we also choose the thermostat relaxation time τ to be unity, the Lyapunov spectrum (based on 10^9 timesteps of length 0.001 each) is:

$$\{\langle\lambda\rangle\}_{\mathrm{eq}} = \{+0.066, +0.000, -0.000, -0.066\}.$$

The spectrum shows the time-reversal symmetry associated with equilibrium. Because the sum of the (time-averaged) exponents vanishes, the various partial sums (corresponding to subspace growth rates) are never negative:

$$\left\{\sum\langle\lambda_{\rm eq}\rangle\right\} = \{+0.066, +0.066, +0.066, +0.000\}.$$

In the simplest nonequilibrium (far-from-equilibrium) case we choose to study here we set $T = 1 + \tanh(q)$. This combination generates a multifractal with an information dimension between 2 and 3 in the four-dimensional phase space. The Lyapunov exponents are:

$$\{\langle\lambda\rangle\}_{\rm neq} = \{0.072_6, 0.0000, -0.091_2, -0.411_0\}.$$

It is important to emphasize that though the four ordinary differential equations generating the flow, as well as the sixteen additional equations describing its sensitivity to perturbations, are all perfectly symmetric in the time, the time-symmetry of the solution is broken by instability, with the Lyapunov exponents no longer occurring in symmetric pairs.

This symmetry breaking has been analyzed in considerable detail for similar systems [20]. It reflects the fact that a flow proceeding forward in time is less unstable (negative Lyapunov sum) than is the time-reversed flow (positive Lyapunov sum) which would violate the Second Law of Thermodynamics. The nonequilibrium Lyapunov sum of all four Lyapunov exponents is necessarily negative, for stability. In the particular case considered here, the one-, two-, three- and four-exponent sums are

$$\left\{\sum\langle\lambda_{\rm neq}\rangle\right\} = \{0.073, 0.073, -0.019, -0.430\}.$$

Linear interpolation, between the two-exponent sum, 0.072_6, and the three-exponent one, -0.018_6, gives the Kaplan–Yorke estimate for the information dimension, $D_{\rm KY} = 2 + \frac{73}{90} \simeq 2.80$. This is a dimensionality reduction of 1.20 below the equilibrium dimensionality of 4.00. In the large-system work described in Ref. [17] dimensionality reductions (from the Lyapunov spectrum, through $D_{\rm KY}$) as large as 34 were observed (in a 578-dimensional phase space).

The information dimension, $D_1 = D_I \simeq D_{\rm KY}$, can also be evaluated, with an uncertainty of order one percent, by simple bin-counting. See Fig. 6. Using 10^9 points separated in time by 1000dt gives the considerably lower estimate $D_I = 2.56$. The entropy-binsize plot, spanning the range from 8^4 bins to 128^4 bins, gives an excellent straight line, $S_1 \propto \ln(\Delta)$. The data show that the Kaplan–Yorke conjecture is simply wrong for this four-dimensional attractor. Evidently the rapid rotation rates of the Lyapunov vectors are responsible for the 10% discrepancy, $D_{\rm KY} \simeq 1.1 D_I$.

The correlation dimension D_2 can also be estimated independently of bin counting, but without such high accuracy. A logarithmic plot of the number of *pairs* of points lying within a distance r of one another increases as $D_2 \ln r$ provided that r is not too large and that the sampling time between successive points is enough for correlations to decay (for a short sampling time the dimensionality of the distribution would be one-dimensional, corresponding to a trajectory). The equilibrium case can be used to test these ideas, for all the dimensions are precisely equal to four. In Fig. 6 we show the variations of all the one- and two-point entropies,

$$S_p \equiv \langle -\ln(\mu_p)\rangle \equiv \left\langle \sum -\mu_p \ln \mu_p \right\rangle.$$

The calculations shown are all based on 10^9 points, separated by 1000 timesteps of d$t = 0.001$ each. The dimensionalities from these data all lie within half a percent of the correct values (1, 2, 3, 4).

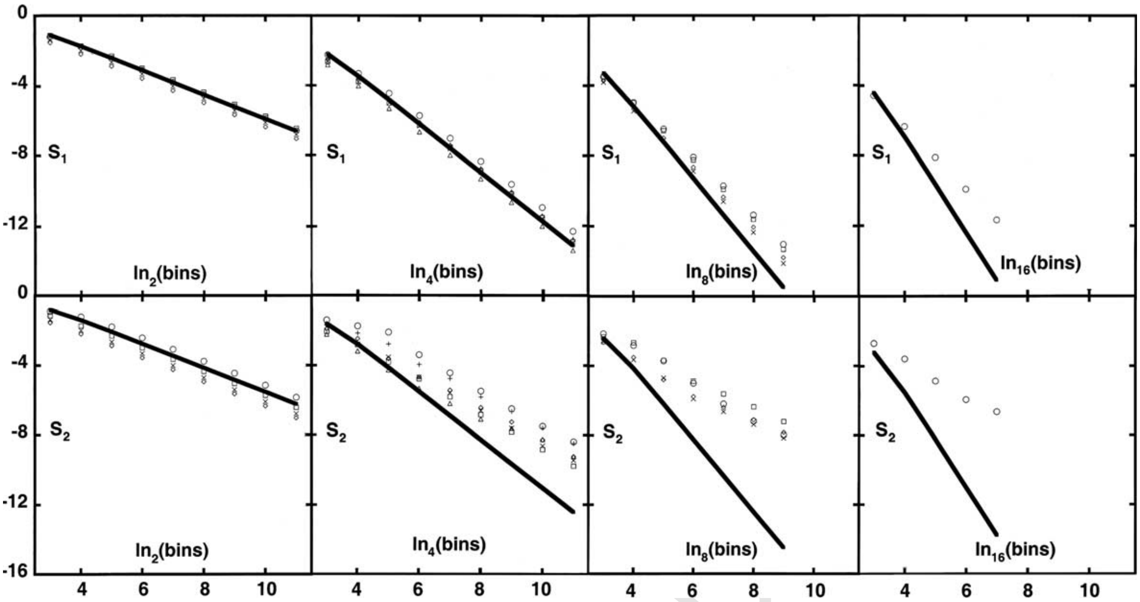

Fig. 6. Dependence of the one-, two-, three- and four-dimensional entropies on the number of bins. The equilibrium (lines) and nonequilibrium (discrete plotting symbols) entropies S_1 and S_2 are compared by using measures proportional to N_k^1 and N_k^2. One billion points, separated by 1000dt were used to generate these data. The minimum and maximum limits for each of the four variables were ± 6. In one, two, three, and four dimensions we used up to 2^{11}, 2^{22}, 2^{27}, and 2^{28} bins, respectively. The logarithms of the numbers of bins are logarithms with bases (2, 4, 8, 16) in (1, 2, 3, 4) dimensions.

The dimensionalities in the nonequilibrium case (See again Fig. 6) reveal some interesting differences. We noticed that the entropy corresponding to the *three*-point measure μ_3 varies in a *non-monotonic* way with the bin size Δ. A simple four-bin example for such a variation can be based on the following bin occupancy numbers:

$$\{1,1,2,0\} \to \{\mu_3\} = \{0.1, 0.1, 0.8, 0.0\}.$$

The entropy S associated with this measure is

$$-\sum \mu_3 \ln \mu_3 = 0.2303 + 0.2303 + 0.1785 + 0.000 = 0.639.$$

Combining the data into pairs (corresponding to coarsening the grid) leads to a (counterintuitive) *increase* in the entropy:

$$\{2,2\} \to \{\mu_3\} = \{0.5, 0.5\} \to S = 0.693.$$

Figs. 7 and 8 summarize the correlation-dimension data for both the equilibrium and nonequilibrium data sets in all 15 of the various subspaces. The equilibrium data (Fig. 7) show that the number of pairs of points in the full four-dimensional phase space and with $\sqrt{q^2 + p^2 + \zeta^2 + \xi^2} < R_{qp\zeta\xi}$ varies as R^4. The four sets of three-dimensional data, corresponding to

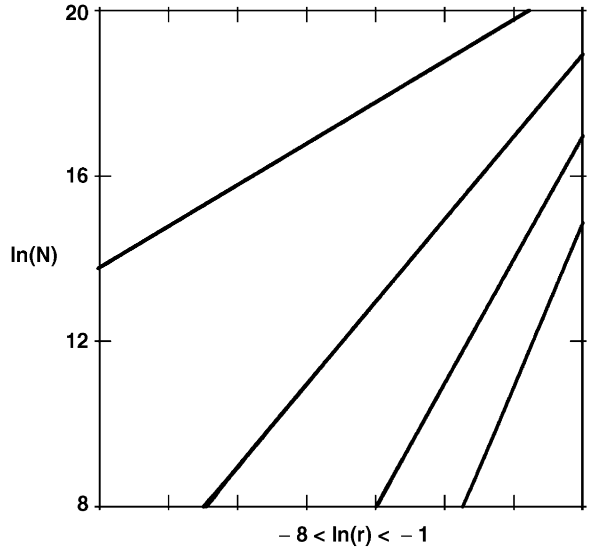

Fig. 7. Dependence of the fifteen equilibrium pair correlations on the bin size. 100,000 data points, separated by intervals of 1000dt, generated the 4,999,950,000 pairs of points contributing to this plot. The slopes of the straight-line portions of the fifteen curves are accurately 1.00, 2.00, 3.00, and 4.00, corresponding to the dimensionalities of the corresponding Gaussian functions. The four one-dimensional sets of data are indistinguishable within the width of the plotting line, as are also the six two-dimensional data sets, and the four three-dimensional data sets.

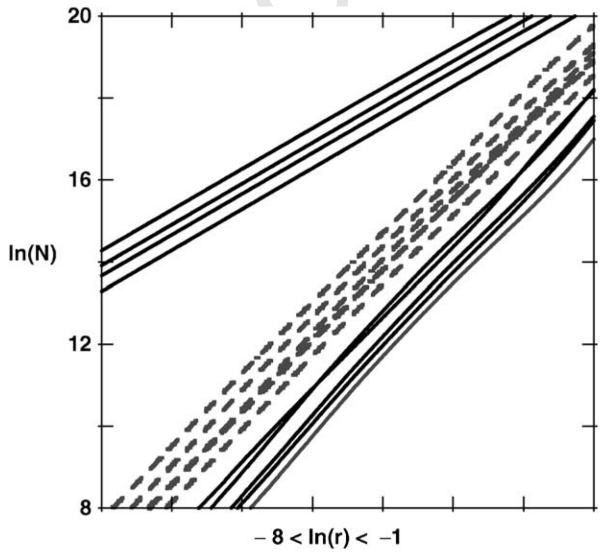

Fig. 8. Dependence of the fifteen nonequilibrium pair correlations on the bin size. 100,000 data points, separated by intervals of 1000dt, generated the 4,999,950,000 pairs of points contributing to this plot. The slopes of these plots correspond (beginning with the one-dimensional data at the top of the figure) to correlation dimensions of 1.00, 1.7_2, 1.8_5, and $\simeq 2$ for the 1, 2, 3, and 4-dimensional subspaces, respectively, with no significant difference between the various subspaces that have the same dimensionality.

$$\sqrt{q^2+p^2+\zeta^2} < R_{qp\zeta}; \quad \sqrt{q^2+p^2+\xi^2} < R_{qp\xi};$$
$$\sqrt{q^2+\zeta^2+\xi^2} < R_{q\zeta\xi}; \quad \sqrt{p^2+\zeta^2+\xi^2} < R_{p\zeta\xi},$$

the six sets of two-dimensional data, and four sets of one-dimensional data are all assembled in Table 1.

The nonequilibrium correlation dimensions are all less than 2. But the full phase-space correlation dimension from pairs of points, 1.8 ± 0.05, does not agree very well with the D_2 estimates from bin-counting. These bin counting results for D_2 are relatively unreliable. Unlike the information dimension, the correlation dimension is sensitive to the number of bins used in the analysis. Strong dimensionality reduction persists in all the subspaces through the six two-dimensional examples. Fig. 9 shows histograms for the one-dimensional spaces, $\ln N_k(q)$ and $\ln N_k(p)$. Though the appearance of these histograms certainly suggests the possibility of a fractal dimension less than unity, we found no significant deviation from $D = 1.00$ for either of them.

Table 1
Equilibrium and nonequilibrium correlation dimensions from cumulative number of pairs

Space	Equilibrium D_2	Nonequilibrium D_2
(q,p,ζ,ξ)	(4.01)	(1.81)
(q,p,ζ), (q,p,ξ), (q,ζ,ξ), (p,ζ,ξ)	(2.98, 2.99, 2.99, 3.00)	(1.93, 1.89, 1.86, 1.90)
(q,p), (q,ζ), (q,ξ), (p,ζ), (p,ξ), (ζ,ξ)	(1.99, 1.99, 1.99, 1.99, 1.99, 1.99)	(1.73, 1.73, 1.75, 1.75, 1.69, 1.77)
(q), (p), (ζ), (ξ)	(1.00, 1.00, 1.00, 1.00)	(0.98, 0.92, 0.98, 0.98)

The first column indicates the space in which the distances between all pairs were determined. The second and third columns are the equilibrium and nonequilibrium pair dimensions D_2. The data are based on 50,000 points with a sampling interval of 10,000 timesteps between successive points.

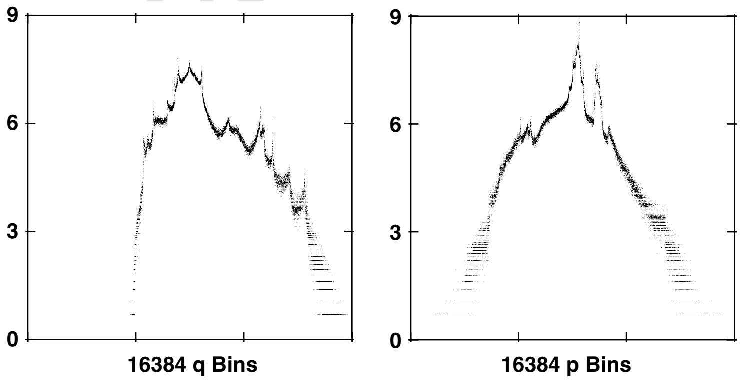

Fig. 9. Logarithms of the probability densities for the nonequilibrium coordinate q and the momentum p. 10^9 points, separated by 1000 timesteps, were used. Bin counting, in the two one-dimensional spaces, suggests information and correlation dimensions in these subspaces quite close to unity. See also the corresponding curve in Fig. 8. The 16,384 bins illustrated here span the range ± 6 for both q and p.

Table 2
The equilibrium Lyapunov exponents $\langle\lambda\rangle$ and their time-averaged projections $\langle(\delta_q^2, \delta_p^2, \delta_\zeta^2, \delta_\xi^2)\rangle$ (top) and the projections weighted with the instantaneous values of the corresponding Lyapunov exponents (bottom)

$\langle\lambda\rangle$	$\langle\delta_q^2\rangle$	$\langle\delta_p^2\rangle$	$\langle\delta_\zeta^2\rangle$	$\langle\delta_\xi^2\rangle$
+0.068	0.141	0.190	0.298	0.371
+0.002	0.306	0.210	0.228	0.256
−0.002	0.177	0.310	0.266	0.248
−0.068	0.377	0.291	0.208	0.124
$\langle\lambda\rangle$	$\langle\lambda\delta_q^2\rangle$	$\langle\lambda\delta_p^2\rangle$	$\langle\lambda\delta_\zeta^2\rangle$	$\langle\lambda\delta_\xi^2\rangle$
+0.068	−0.002	+0.014	+0.013	+0.043
+0.002	+0.004	−0.011	+0.008	+0.002
−0.002	−0.002	+0.002	−0.004	+0.001
−0.068	−0.040	−0.013	−0.011	−0.004

Note that the row sums are unity at the top, and $\langle\lambda\rangle$ at the bottom. These data apply to the *equilibrium* oscillator, with $\epsilon = 0$ and correspond to 10^9 timesteps of 0.001 each. These data are all time averages.

6. Kaplan–Yorke Conjecture for Subspaces

Kaplan and Yorke's conjecture has a strong intuitive basis. It is certainly "obvious" that the dimension of a strange attractor is the same as the dimensionality of an object which neither grows nor shrinks over time. We have seen that fluctuations in the Lyapunov vectors' directions can lead to ten percent errors in the estimate. Nevertheless, it is tempting (if not irresistible) to apply the Kaplan–Yorke idea in subspaces of the full phase space, in order to estimate the projected information dimensions there. We set about to do this.

See Tables 2 and 3 for the Lyapunov vector projections. In work with the many-body ϕ^4 model [16] we used the exact relation that the instantaneous subspace growth rate corresponding to the set of Lyapunov vectors $\{\lambda_i\}$ in the full phase space, is given by the weighted sum, $\sum\lambda_i\cos^2(\theta_i)$, where $\cos(\theta_i)$ is the projection of the phase-space vector δ_i into the subspace. We estimated the

Table 3
The *nonequilibrium* Lyapunov exponents $\langle\lambda\rangle$ and their time-averaged projections $\langle(\delta_q^2, \delta_p^2, \delta_\zeta^2, \delta_\xi^2)\rangle$ (top) and the projections weighted with the instantaneous values of the corresponding Lyapunov exponents (bottom)

$\langle\lambda\rangle$	$\langle\delta_q^2\rangle$	$\langle\delta_p^2\rangle$	$\langle\delta_\zeta^2\rangle$	$\langle\delta_\xi^2\rangle$
+0.072	0.098	0.112	0.257	0.533
+0.000	0.227	0.181	0.308	0.284
−0.091	0.293	0.363	0.237	0.107
−0.410	0.382	0.343	0.198	0.077
$\langle\lambda\rangle$	$\langle\lambda\delta_q^2\rangle$	$\langle\lambda\delta_p^2\rangle$	$\langle\lambda\delta_\zeta^2\rangle$	$\langle\lambda\delta_\xi^2\rangle$
+0.072	−0.013	−0.001	+0.028	+0.058
+0.000	+0.005	−0.007	+0.018	−0.015
−0.091	−0.010	−0.047	−0.023	−0.012
−0.410	−0.168	−0.137	−0.088	−0.018

Note that the row sums are unity at the top, and $\langle\lambda\rangle$ at the bottom. All these data apply to the *nonequilibrium* oscillator, with $\epsilon = \tau = h = 1$ and correspond to 10^9 timesteps of 0.001 each. These data are all time averages.

information dimension of the subspace attractor from the sum $\sum \cos^2(\theta_i)$ of weights required for the projected growth rate to vanish. This idea is correct in the event that the orientations of the vectors are random, with $\cos^2(\theta_i)$ equal to the inverse number of vectors. In the many-body systems studied in Ref. [16] it was observed that the projections became increasingly uniform as the system size increased. A four-dimensional phase space is a demanding test of this idea. The failure here of the Kaplan–Yorke conjecture in the full phase space was unexpected.

The failure of Kaplan–Yorke in four dimensions led us to try to apply an idea like theirs in lower-dimensional subspaces of the full space, where convergence is enhanced. Unfortunately, the data in Table 2 indicate that this approach fails completely for the thermostatted oscillator. The projections of the vectors vary considerably about the random value, 0.25, with minimum/maximum values of 0.12/0.38. The projected growth rates contain a surprise (which we found with other oscillator models as well as with some few-body subspace projections of the many-body ϕ^4 dynamics). *The largest most positive Lyapunov exponent can have a negative time-averaged projection in some subspace directions.* Consider, for example, our oscillator problem projected into the coordinate q subspace. Bin counting results show that the information and correlation dimensions in q space are not significantly different to 1.00. But the instantaneous value of λ_1, where the time average $\langle \lambda_1 \rangle$, includes, at each instant, multiplication by its corresponding unit vector δ_1 has, on the average, a *negative* projection in q space. The data in Tables 2 and 3 show that there is no consistent way to obtain accurate information dimensions in the various subspaces. We conclude that at best the Kaplan–Yorke procedure can work well in subspaces only in high-dimensional systems. Provided that a long trajectory could be replaced by several thousand shorter ones (and this could be checked numerically) presentday computers *might* be able to characterize attractors in a six-dimensional space (with 10^{12} bins). There is no forseeable chance that these ideas can be checked in many-dimensional phase spaces for which bin counting is, and always will be, impossibly difficult.

The present work shows that the Kaplan–Yorke conjecture is flawed in the full phase space. The information dimension of the full phase-space attractor, as estimated by bin counting, is 2.56. The Kaplan–Yorke prediction is considerably, and significantly, higher, 2.80. Results for the correlation dimension are inconclusive. The bin-counting value in the full phase space is 1.55, but with an uncertainty of ± 0.2. The dimension estimated from pair enumerations is 1.81.

7. Conclusion

The deterministic, continuous, dissipative, doubly-thermostatted oscillator problem is a useful prototype for understanding multifractal distribution functions far from equilibrium. It lies near the borderline for presentday computational feasibility. A very similar oscillator model leads exactly to Clausius' version of the Second Law of Thermodynamics,

$$\langle -\mathrm{d}S_{\mathrm{ext}}/\mathrm{d}t \rangle = \langle (1/T)\mathrm{d}Q/\mathrm{d}t \rangle < 0.$$

This inequality is an automatic consequence of Nosé–Hoover mechanics, where the specified reservoir temperatures are constants of the motion. In the case that temperature varies Clausius' inequality is satisfied with the definition:

$$\zeta_{NH} \equiv [(p^2/mkT) - 1]/\tau^2,$$

but is *not* automatically satisfied with the alternative:

$$\zeta_{NH} \equiv [(p^2 - mkT)/mkT_0]/\tau^2.$$

The equilibrium case, with its four-dimensional Gaussian distribution, can be used to evaluate the accuracy of algorithms. Our results indicate that the correlation dimension, which is considerably simpler to evaluate than the bin-counting dimensions, is a good characterizer of fractals, with the numerical pair-counting and bin-counting versions of D_2 not inconsistent with one another. For this model all six of the two-dimensional projections of the attractor had similar Kaplan–Yorke dimensions and similar correlation dimensions. This finding suggests a rapid rotation in phase space, tending to make the attractor relatively isotropic and homogeneous, even for a few-dimensional phase space. The model has also a particularly interesting feature, a contracting time-averaged projection of the four-dimensional dynamics into the one-dimensional coordinate space. This indicates that there is no simple analog of the Kaplan–Yorke conjecture for subspaces, at least for the present model system. The finding that the Kaplan–Yorke conjecture is inaccurate in the full phase space was a major surprise to us.

Acknowledgements

WGH's work in Carol Hoover's Methods Development Group at the Lawrence Livermore National Laboratory was performed under the auspices of the United States Department of Energy through University of California Contract W-7405-Eng-48. Julian Codelli's work at the Department of Applied Science was sponsored by the Academy of Science (Concord, New Hampshire) through their summer REAP program for exceptional students. He is now with the University of California at Berkeley. HAP acknowledges the support of the Austrian Fonds zur Förderung der Wissenschaftlichen Forschung through Grant P15348-PHY. We are all particularly grateful to the Erwin Schrödinger Institute in Vienna for sponsoring a workshop under the STOCHDYN program at which we were able to discuss and present some of these results. We thank Harald Oberhofer and Jacobus van Meel for useful discussions there.

References

[1] Nosé S. J Chem Phys 1984;81:511.
[2] Nosé S. Mol Phys 1984;52:255.
[3] Hoover WG. Phys Rev A 1985;31:1685.
[4] Posch HA, Hoover WG, Vesely FJ. Phys Rev A 1986;33:4253.
[5] Moran B, Hoover WG, Bestiale S. J Stat Phys 1987;48:709. For a more mathematical approach to this problem see Ref. [8].
[6] Holian BL, Hoover WG, Posch HA. Phys Rev Lett 1987;59:10.
[7] Chernov NI, Eyink GL, Lebowitz JL, Sinai YG. Phys Rev Lett 1993;70:2209.
[8] Ruelle D. J Stat Phys 1999;95:393.
[9] Hoover WmG. Time reversibility, computer simulation, and chaos. Singapore: World Scientific; 1999.
[10] Posch HA, Hoover WG. Phys Rev E 1997;55:6803.

[11] Hoover WG. Computational statistical mechanics. New York: Elsevier; 1991.
[12] Posch HA, Hoover WG. Nonequilibrium molecular dynamics of classical fluids. In: Teixeira-Dias JJC, editor. Molecular liquids: new perspectives in physics and chemistry. Amsterdam: Kluwer; 1992. p. 22.
[13] Ruelle D. Phys Today 2004;57(5):48.
[14] Aoki K, Kusnezov D. Phys Lett A 2000;265:250.
[15] Aoki K, Kusnezov D. Phys Rev E 2003;68:056204.
[16] Hoover WmG, Aoki K, Hoover CG, De Groot SV. Physica D 2004;187:253.
[17] Posch HA, Hoover WmG. Physica D 2004;187:281.
[18] Hoover WG. Comput Methods Sci Tech (Poznán) 1997;3:19.
[19] Chhabra A, Jensen RV. Phys Rev Lett 1989;62:1327.
[20] Hoover WmG, Hoover CG, Posch HA. Comput Methods Sci Tech (Poznán) 2001;7:55.